THE JOURNAL OF PHYSICAL CHEMISTRY B

ARTICLE

pubs.acs.org/JPCB

Molecular Dynamics Simulations of Carbon Dioxide and Water at an Ionic Liquid Interface

Marcos E. Perez-Blanco and Edward J. Maginn*

Department of Chemical and Biomolecular Engineering, University of Notre Dame, 182 Fitzpatrick Hall, Notre Dame, Indiana 46556, United States

Supporting Information

ABSTRACT: The ionic liquid−carbon dioxide system is of interest because ionic liquids (ILs) have potential to be used for carbon dioxide capture. Because water will be present in a real carbon dioxide capture operation, the interaction between water and the IL is also of interest. Classical molecular dynamics simulations have been used to study the IL 1-*n*-butyl-3-methylimidazolium bis(trifluoromethylsulfonyl)imide (bmim-Tf_2N) at the interface with vacuum as well as with carbon dioxide, water, or both present in the system. Density and orientational ordering of the ionic liquid molecules at the interface was not significantly altered by the presence of either carbon dioxide or water. The structure of the liquid solutions in the pseudobulk region in the center of the slab was studied using metrics of pairwise association such as radial distribution functions. At the interface, there is an increased density of cation−anion association. When carbon dioxide is present, it forms a dense layer on the surface, and the cation−anion associations at the interface are disrupted, with a corresponding decrease in surface tension. Water slows down the diffusion of the ions as well as carbon dioxide in the bulk. Water has little effect, however, on the interfacial transport dynamics of carbon dioxide.

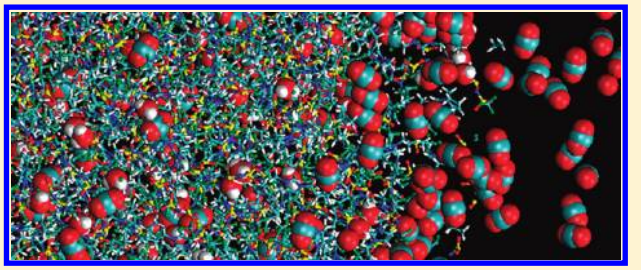

INTRODUCTION

Ionic liquids (ILs) have been suggested as possible solvents for CO_2 capture processes due to the fact that some ILs have high capacities and selectivities for CO_2 compared with other gases such as N_2, H_2, and O_2.[1,2] There are an enormous number of possible ILs, so it is not practical to attempt to measure the thermodynamic and transport properties for all of them. Molecular-based computer simulations could be used to predict properties of interest and identify ILs for experimental testing, thereby avoiding the impracticality of performing experiments on a large number of different liquids. Molecular simulations have the added benefit that they can provide detailed atomistic-level information that may be difficult if not impossible to measure from experiment.

In a previous publication,[3] the 1-*n*-butyl-3-methylimidazolium bis(trifluoromethylsulfonyl)imide (bmim-Tf_2N) interface with vacuum and the bmim-Tf_2N/CO_2 interface was studied by molecular dynamics (MD) simulation, with the goal of understanding the microscale behaviors that influence thermodynamic and transport properties relevant to CO_2 capture. Properties such as orientation of molecules, density behavior with respect to the surface normal, and relative population of different molecular species at the surface all affect the dynamics of adsorption of gas molecules and absorption into the bulk. These properties were all investigated using MD simulations.

Work done by other researchers on IL/vacuum systems was in agreement with what we previously observed.[3] For example, Pensado et al.[4] simulated the 1-*n*-hexyl-3-methylimidazolium bis(trifluoromethylsulfonyl)imide (hmim-Tf_2N) interface with vacuum and obtained similar results for properties such as density ordering and molecular orientation. Balasubramanian and colleagues[5] simulated the interface of C_3C_1im-, C_3C_3im-, C_5C_1im-, and C_5C_5im-Tf_2N with vacuum. The observed orientation of the alkyl chains and of the imidazolium ring is in agreement with our previous study of bmim-Tf_2N.[3]

MD has also been used by Dang and colleagues[6,7] to simulate bmim-PF_6/CO_2 and bmim-BF_4/CO_2 systems. In addition to reporting characteristics of the density profile that are in agreement with other computation studies, the potential of mean force (PMF) for interfacial crossing of CO_2 was calculated for both ILs. The PMFs show similar features to the PMF reported in our previous work,[3] although the actual energies are not in agreement, possibly because different ILs were used.

X-ray reflectivity experiments by Nishi et al.[8] show that underneath the liquid surface, the cations and anions form alternating layers, which is in agreement with computational results. Roscioli and Nesbitt[9] have reported molecular scattering experiments using CO_2 on bmim-Tf_2N and bmim-BF_4 IL surfaces. According to those experiments, ∼70% of incoming CO_2 molecules are "trapped" by the IL surface, with the remainder being elastically scattered. This is consistent with our calculated interfacial residence time distributions (RTDs).[3]

Received: April 25, 2011
Revised: July 28, 2011
Published: July 29, 2011

Because H_2O will be present in the flue gas from which CO_2 is to be captured, the behavior of H_2O in an IL/CO_2 system is of interest. In particular, it would be useful to know how the presence of H_2O alters the interfacial ordering behaviors of the IL and CO_2 and how interfacial transport dynamics and bulk diffusion are affected.

Interfacial systems of dimethylimidazolium chloride (dmim-Cl) and H_2O have been simulated by Lynden-Bell and colleagues.[10,11] Their studies show that H_2O accumulates toward the outside of the vapor/liquid interface. Also, for the lower concentrations of H_2O, the H_2O molecules in the interfacial region were observed to be oriented so that one of the OH bonds pointed outward.

The effect of H_2O on the bulk behavior of ILs has been studied using MD by Margulis and colleagues.[12] Diffusive and rotational dynamics are both accelerated by the presence of H_2O but only slightly. Moreno et al.[13] have studied the interaction between H_2O and bmim-BF_4 using MD simulations. They report that at low H_2O concentrations diffusion is actually slower than that in the pure IL for one of the force fields used. The dynamics speed up as the concentration of H_2O is increased. The anomalous result is attributed to the nanoscale organization of the mixtures with low H_2O content. It was observed that most of the H_2O molecules at mole fractions <0.2 are either isolated or in pairs and that this fails to disrupt the IL ion−ion network, so diffusion is not increased. Also, Hanke and Lynden-Bell[14] have observed that at low mole fractions of H_2O (<0.75) most of the H_2O molecules were isolated, whereas at higher mole fractions the H_2O molecules formed a "percolating network" throughout the IL. Correspondingly, diffusion is nearly unaffected at lower concentrations but then begins to increase rapidly when the mole fraction of H_2O reaches 0.75. Voth and colleagues[15] have observed a similar tendency for mixtures of 1-*n*-octyl-3-methylimidazolium nitrate (omim-NO_3) and H_2O. At lower H_2O concentrations, a nanostructured state was observed in which H_2O primarily interacts with NO_3. When the concentration of H_2O was increased, H_2O−H_2O interactions dominated, and the IL−IL network was disrupted.

In this work, a third component, H_2O, was added to the bmim-Tf_2N/CO_2 interfacial system. The properties that are of primary interest include bulk and interfacial transport dynamics. Additionally, molecular density ordering and orientational preference at the interface was calculated. The behavior of intermolecular associations at the interface, and, in particular, the manner in which those between the cation and anion were altered by the presence of solute molecules, was studied. The behavior of H_2O in the IL has been studied by examining hydrogen bonding and the degree to which H_2O associates with the IL and with itself.

SIMULATION METHODS

A two phase interfacial system was simulated, consisting of the IL (bmim-Tf_2N) in the liquid phase and either vacuum or H_2O vapor, CO_2, or both in the gas phase. The structure of bmim-Tf_2N is shown in Figure 1. The atom labels shown in the Figure are used elsewhere to refer to these atoms, followed by the molecule containing the atom in parentheses. For example, the terminal carbon of the butyl chain of bmim would be C10(+), the sulfurs of Tf_2N would be S(−), the oxygen of H_2O would be O(H_2O), and so on.

A classical MD force field was used to model the inter- and intramolecular interactions, where the total potential energy is

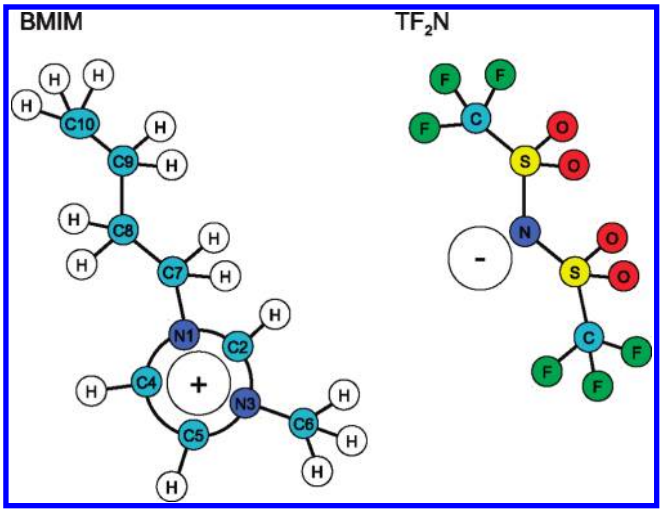

Figure 1. Structure of bmim-Tf_2N.

given by eq 1. Lennard-Jones and Coulombic terms are used for nonbonded interactions, harmonic potentials for molecular bonds and angles, and CHARMM-style potentials for molecular dihedrals.

$$v(r) = \sum_{\text{bonds}} k_r(r - r_0)^2 + \sum_{\text{angles}} k_\theta(\theta - \theta_0)^2 + \sum_{\text{dihedrals}} k_\chi[1 + \cos(n_0\chi - \delta_0)] + \sum_{i=1}^{N-1}\sum_{j=i+1}^{N}\left(4\varepsilon_{ij}\left[\left(\frac{\sigma_{ij}}{r_{ij}}\right)^{12} - \left(\frac{\sigma_{ij}}{r_{ij}}\right)^{6}\right] + \frac{q_i q_j}{r_{ij}}\right) \quad (1)$$

N is the number of atoms, $\varepsilon_{i,j}$ and $\sigma_{i,j}$ are the Lennard-Jones parameters for atom pair (i,j), and q_i is the (fixed) partial charge on atom i.

The parameters for bmim were taken from the work of Cadena et al. and include parameters from CHARMM,[16,17] whereas parameters for Tf_2N were taken from the force field developed by Padua and Lopes.[18] The TraPPE model for CO_2, developed by Potoff and Siepmann,[19] is a three-site model with partial charges on the atom centers. It has been shown to give excellent thermodynamic predictions, and so it was chosen for this work. H_2O was simulated with the simple point charge (SPC) water potential.[20] The force fields for CO_2 and H_2O were modified slightly to make them fully flexible, corresponding with the all-atom, fully flexible bmim-Tf_2N force field. The LAMMPS MD software[21,22] was used to perform the simulations.

All systems contained 368 IL pairs, which composed the IL slab with vapor space on either side. The plane of the slab was parallel to the *xy* plane, so that the *z* axis was normal to the interface. A more detailed description of the simulation methods and procedures for generating the IL slab configuration may be found in our previous publication.[3]

The IL/H_2O system additionally contained 96 H_2O molecules, the IL/CO_2 system contained 192 CO_2 molecules, and the IL/H_2O/CO_2 system contained 96 H_2O molecules and 192 CO_2 molecules. For the IL/H_2O and IL/CO_2 systems, the H_2O or CO_2 molecules started out in the vapor space. Simulations were run for a total of 12 ns for the absorption of the gas into the

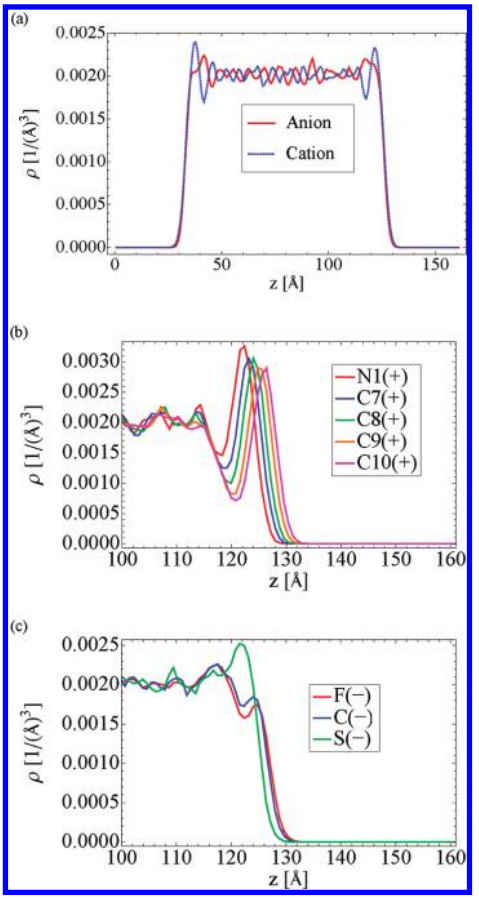

Figure 2. Density profiles for the IL/vacuum system at 350 K.

liquid to get close to equilibrium. For the case of the IL/H_2O/CO_2 system, the configuration of the IL/H_2O system was taken after 12 ns of simulation (during which H_2O was absorbed into the IL), and CO_2 was then added to the gas phase. The system was run for an additional 12 ns during which time the CO_2 was absorbed into the liquid.

Every 1 ps, atomic coordinates were written to file, creating a simulation trajectory in 1 ps timeframes. Postprocessing code was developed to compute various aspects of the bulk and interfacial properties from the output trajectories. These analyses are described in the next section.

■ ANALYSIS OF RESULTS

Molecular Structure at the Interface. Normalized density profiles with respect to the z axis of various molecules and atoms were created. The details of the computations for these analyses can be found in a previous publication.[3] Additionally, correlation values for the density profiles were computed as shown in eq 2.

$$C(\rho_a, \rho_b) = \frac{\sum_{z,lq}((\rho_a(z) - P_a)\cdot(\rho_b(z) - P_b))}{\sqrt{\sum_{z,lq}(\rho_a(z) - P_a)^2}\cdot\sqrt{\sum_{z,lq}(\rho_b(z) - P_b)^2}} \quad (2)$$

$C(\rho_a,\rho_b)$ is the correlation value between a pair of density profiles $\rho_a(z)$ and $\rho_b(z)$. The z,lq subscript indicates that the summations are performed only over all z values that are in the liquid phase. P_a and P_b are the average values of the profiles in the liquid region.

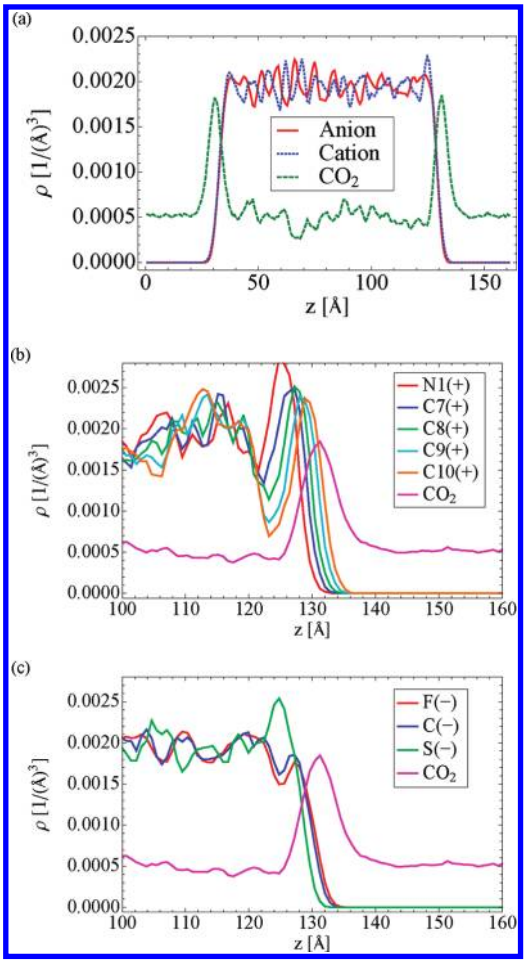

Figure 3. Density profiles for the IL/CO_2 system at 350 K.

The correlation value indicates to what degree two profiles are correlated as a function of z. Perfect correlation gives a value of +1.0, whereas exact anticorrelation gives a value of −1.0.

For comparison with the results of the IL with H_2O or CO_2 systems, density profiles for the IL/vacuum system at 350 K are shown in Figure 2. The density profiles for the anion and cation are shown in Figure 2a, for selected atoms of the cation in Figure 2b, and for selected atoms of the anion in Figure 2c. These profiles are consistent with previous results at 400 K.[3] The correlation value of the cation and anion density profiles is −0.51, indicating a significant amount of anticorrelation between the cation and anion density.

The density profiles for the IL/CO_2 system are shown in Figure 3. Figure 3a shows the density profiles for the cation, anion, and CO_2, and Figure 3b,c shows density profiles of selected atoms of the cation and anion, respectively. They are very similar to the 400 K profiles previously computed.[3] Interfacial ordering tendencies, density oscillations in the pseudobulk region, molecular density, and orientational ordering are very similar to the IL/vacuum case. The correlation value between the cation and anion density profiles is −0.30, which indicates a smaller anticorrelation than that for the IL/vacuum system at 350 K. It appears that the CO_2 has a randomizing effect on the interior "pseudo-bulk" region.

CO_2 demonstrates a tendency to form a high density adsorbed layer on the surface of the IL. Therefore, it is not surprising that

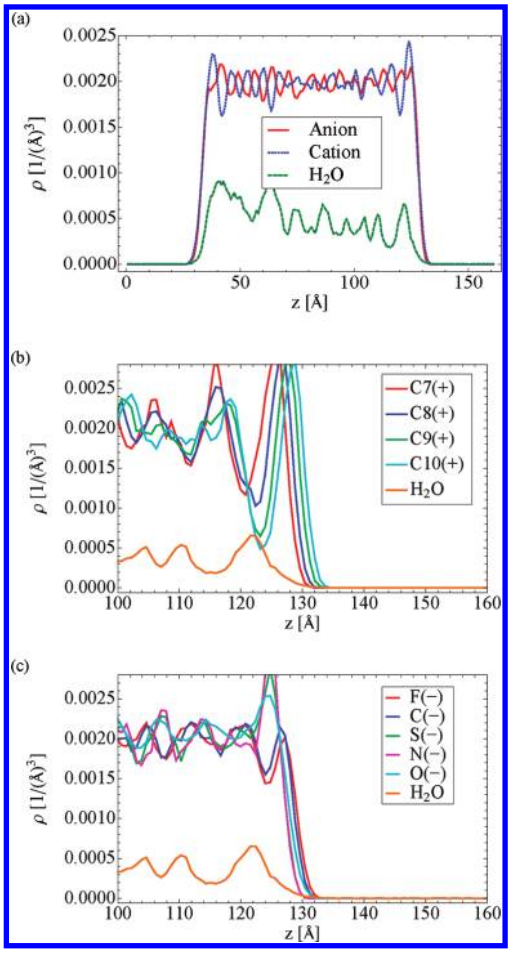

Figure 4. Density profiles for the IL/H_2O system at 350 K.

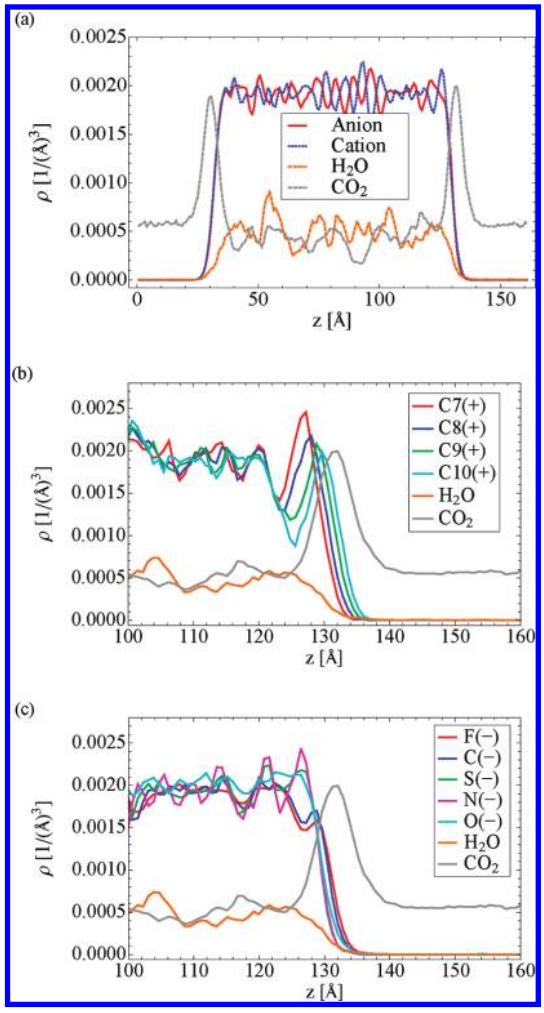

Figure 5. Density profiles for the IL/H_2O/CO_2 system at 350 K.

the molecular scattering experiments performed by Roscioli and Nesbitt[9] show that there is a strong tendency for CO_2 to stick to the IL surface. Furthermore, they observed that the fraction of CO_2 trapped by the surface follows a trend (as a function of the different ILs used) that increases with the enthalpy of solvation but does not follow the Henry's Law constant. On the basis of these observations, they suggest that the surface adsorption results from the strength of IL−CO_2 interactions, whereas solubility is related to free volume in the IL. This would confirm the explanation proposed in our previous publication for why the CO_2 adsorbs onto the surface at a much higher density than in the bulk: it can form strong (VdW and possibly quadrupole-charge) interactions with the surface, without the energy cost of expanding the liquid solution.

The density profiles for the IL/H_2O system at 350 K are shown in Figure 4. The density profiles for the anion, cation, and H_2O are shown in Figure 4a, for selected atoms of the cation in Figure 4b and for selected atoms of the anion in Figure 4c. Note that the H_2O profile shows fluctuations and is not completely symmetric, as would be expected for a fully equilibrated system. Over the last several nanoseconds of the 12 ns simulation, the profile did not change significantly. The average was taken over the last 1 ns of the simulation. Longer averaging may result in a smoother density profile, but the overall water concentration is representative of the equilibrium value.

The gross features of the density profiles are similar to the IL/vacuum and IL/CO_2 cases, suggesting that the H_2O actually has very little effect on the density and molecular orientation at the interface. The density profiles and angular distribution plots (not shown) indicate that the alkyl tails, imidazolium ring, and CF_3 groups are exhibiting the same ordering behavior as the pure IL. However, the density correlation value for the cation and anion is −0.76, which shows that H_2O increases anticorrelation in the system, suggesting that H_2O is imposing an additional structure on the IL.

H_2O does not adsorb at the surface but instead dissolves in the interior of the slab. This is consistent with the PMFs reported by Dang and Wick[7] for interfacial crossing of H_2O. These energy profiles do not have a minimum at the interface but decrease more or less steadily going from the gas to liquid phase.

It can be seen from the plot of the density profile of the cation atoms that the H_2O avoids the outermost region of the interface, which is populated with alkyl tails. Instead, there is a small peak in H_2O density just below the peak in density of the anion oxygens. (See Figure 4c.) It appears that the polar H_2O molecules prefer the negatively charged oxygens of the anion (with which they can hydrogen bond) to the nonpolar alkyl tails of the cation. In contrast, the larger but nonpolar CO_2 strongly accumulates in the outer region of the interface, where it can maximize van der Waals interactions with the IL without disrupting the cation−anion interactions.

Figure 5a shows the density profile for the cation, anion, H_2O, and CO_2 for the IL/H_2O/CO_2 system. Figure 5b shows the

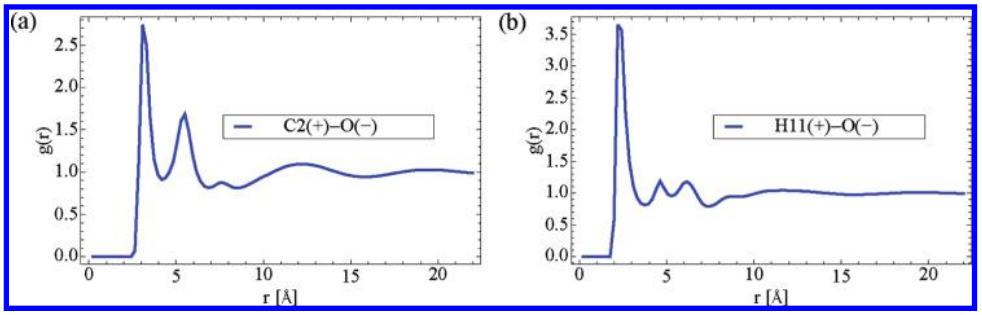

Figure 6. Radial distribution functions in the pseudobulk region of the IL/vacuum system.

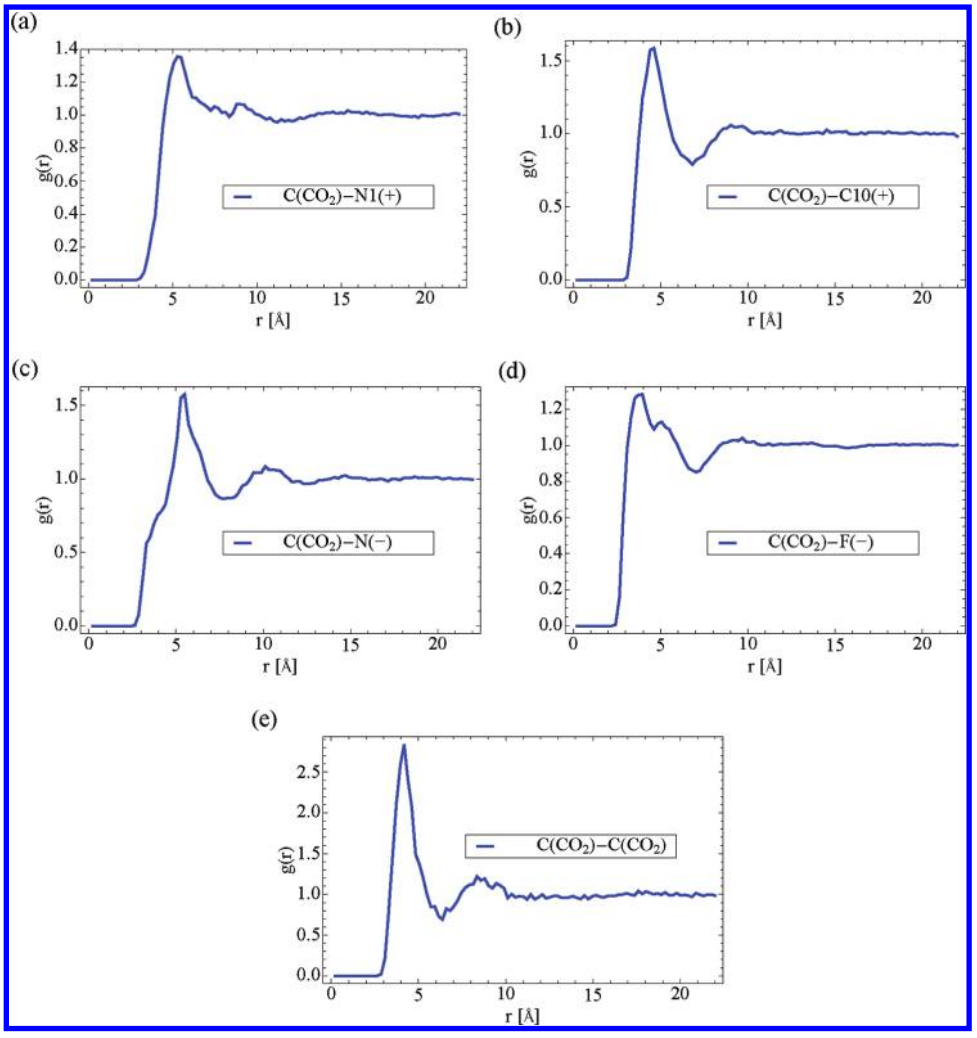

Figure 7. Radial distribution functions around $C(CO_2)$ in the pseudobulk region of the IL/CO_2 system.

density profile of selected atoms of the cation, and Figure 5c shows the density profile of selected atoms of the anion. The correlation value for the cation−anion density profiles drops to −0.55, which shows that CO_2 has a "randomizing" effect that opposes the ordering induced by H_2O. The CO_2 still exhibits a tendency to adsorb at the interface with the IL. Relative to the IL/vacuum and IL/H_2O cases, the interfacial ordering tendencies are not greatly affected.

Structure of the Liquid. To understand the structure and ordering of the IL and IL solutions, various site−site radial distribution functions were computed for atoms in the "pseudo-bulk" region, which was defined as the interior portion of the slab going from 60 to 100 Å in z. Figure 6a shows the RDF for the C2(+)−O(−) pair, and Figure 6b shows the RDF for the H11(+)−O(−) pair in the IL−vacuum system. The sharp peak in both RDFs at about 3 to 4 Å indicates that the cation and anion associate strongly between these two regions, which have relatively high charge density.

Figure 7 shows the RDF for various atoms around the $C(CO_2)$ center for the IL-CO_2 solution. There is no strong association of CO_2 with either the cation or anion or with itself.

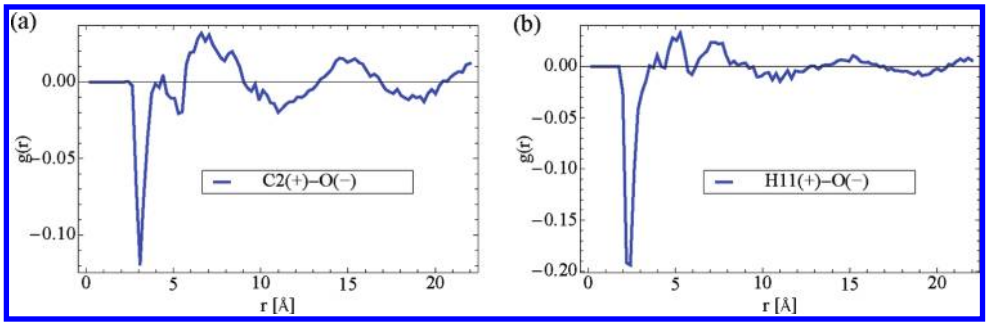

Figure 8. RDF difference plots for the pseudobulk region of the IL/H_2O system.

To illustrate the effect of an additional component in solution on the RDF of several selected pairs, we subtracted the RDF of a pair without the component present in solution from the RDF of the same pair with the component present. Figure 8 shows difference plots when the RDF of the IL/vacuum system is subtracted from the same RDF of the IL/H_2O system for the C2(+)−O(−) and H11(+)−O(−) pairs. There is a small effect of the primary peaks being decreased in the C2(+)−O(−) and H11(+)−O(−) radial distributions. These effects are likely the result of the H_2O dipoles exhibiting charge dipole interactions with the IL ions, screening the charge−charge interactions between the ions.

Figure 9 shows the RDF for the O(H_2O) with various sites in the IL/H_2O system. Figure 9a,b shows that H_2O associates more with the positively charged N1 of the cation than with the nonpolar C10 of the cation. Note the O(H_2O)−O(−) RDF in Figure 9c, which has a strong peak in the first solvation shell at just under 3 Å. This suggests a strong association between H_2O and the oxygen atoms of the anion, which is consistent with previous results.[23−25] Also note the H_2O−H_2O RDF in Figure 9e, which exhibits an extraordinarily high primary peak. This behavior is not seen for the CO_2−CO_2 RDF in the IL/CO_2 system. The RDF for bulk H_2O using various H_2O models has been computed by Mark and Nilsson,[26] and the primary peak is much lower. The high peak observed in the IL/H_2O system indicates a strong correlation between neighboring H_2O molecules, even in the dilute solution, which suggests that the H_2O molecules are paired or in clusters.

Figure 10 shows various RDF difference plots obtained by subtracting the RDF in the IL/CO_2 system from the RDF in the IL/H_2O/CO_2 system. Compared with the IL/CO_2 case, the peak of the C(CO_2)−N3(+) RDF is lower, and the C-(CO_2)−C10(+) peak is higher. This may be because the polar H_2O is displacing the CO_2 from the charged ring and instead the CO_2 associates with the nonpolar alkyl chain. There is very little effect on the C(CO_2)−anion RDFs. Also, the primary peak of the C(CO_2)−C(CO_2) RDF decreases when H_2O is added, showing that the degree of CO_2 association with itself is reduced by the presence of H_2O.

Intermolecular Contacts. One type of intermolecular interaction that is common in polar and charged systems is the hydrogen bond. To test for the existence of hydrogen bonds, we used the following criteria. If a hydrogen bond donor (D) and acceptor (A) were within a 3.3 Å radius and the angle between DH−A was >145°, then the DH−A group was counted as a hydrogen bond. Using these criteria, very few hydrogen bonds were found. The hydrogen bond data had poor statistics and provided little useful information.

However, there is the possibility of close association between various molecules occurring in solution that does not meet the criteria for a formal hydrogen bond. These associations will be referred to as contact pairs (CPs). To study the behavior of CPs, we identified atom pairs (that were on different molecules) that were within a 3.3 Å radius as atomic contact pairs (aCPs). See Figure 11 for a schematic showing the definition of an aCP. The total number of aCPs per frame (averaged over all frames) was computed. The aCP numbers are reported as a percentage of the number of pairs that would be counted assuming a 1:1 pairing between all atoms of a given pair type.

In some cases, it is possible that there could be more than one aCP (of a given pair type) identified between the same pair of molecules. Including both of the aCPs would lead to double counting. To avoid double counting and find the "true" number of molecule-to-molecule contact pairs (mCPs), a count was computed where multiple aCPs between the same two molecules were counted as one mCP. If the number of aCPs is higher than the number of mCPs, then this indicates that pairs of molecules are indeed exhibiting more than one aCP per pair. As with the aCPs, the mCP numbers are reported as percentages of the number that would result from 1:1 pairing.

The position of a CP in z was defined as the midpoint of the vector connecting the contact pair. Profiles in z of the density of aCPs and mCPs were created. Also, the angle (θ) between the pair vector connecting two atoms of an aCP and the interface normal (z vector) was computed. (See Figure 11.) Distribution plots, in two dimensions of z position and θ, were created for the aCPs only. In these plots, the distribution value (dependent variable) was scaled by 1/sin (θ) to cancel out sin(θ) $\partial\theta$ $\partial\phi$ (surface element of a unit sphere), which is the probability that a vector with an isotropically random orientation will be at a given angle θ from the z axis. When this scaling is used, the random orientation should give a uniform distribution in θ. This makes it easier to identify preferential orientational tendencies, which more clearly stand out from a uniform distribution.

The C2(+)−O(−) aCP and mCP counts ware quite large in the IL/vacuum system, at 131.9 and 114.5%, averaged over the entire trajectory. Note that both of these values are higher than 100%. The count of the mCPs shows that the C2(+) is sometimes associating with more than one anion. The aCP count is even higher because the C2(+) is sometimes associating with two or more of the oxygen atoms on the same anion. These CP values correspond with the degree of interaction indicated by the C2(+)−O(−) RDF.

The density profiles for CP centers and the z-angle distribution plot for the aCP vector are shown in Figure 12. There is a strong tendency for these associations to occur with a higher density at the interface. The z-angle distribution plot shows that at the interface these interactions are mostly in the interfacial plane.

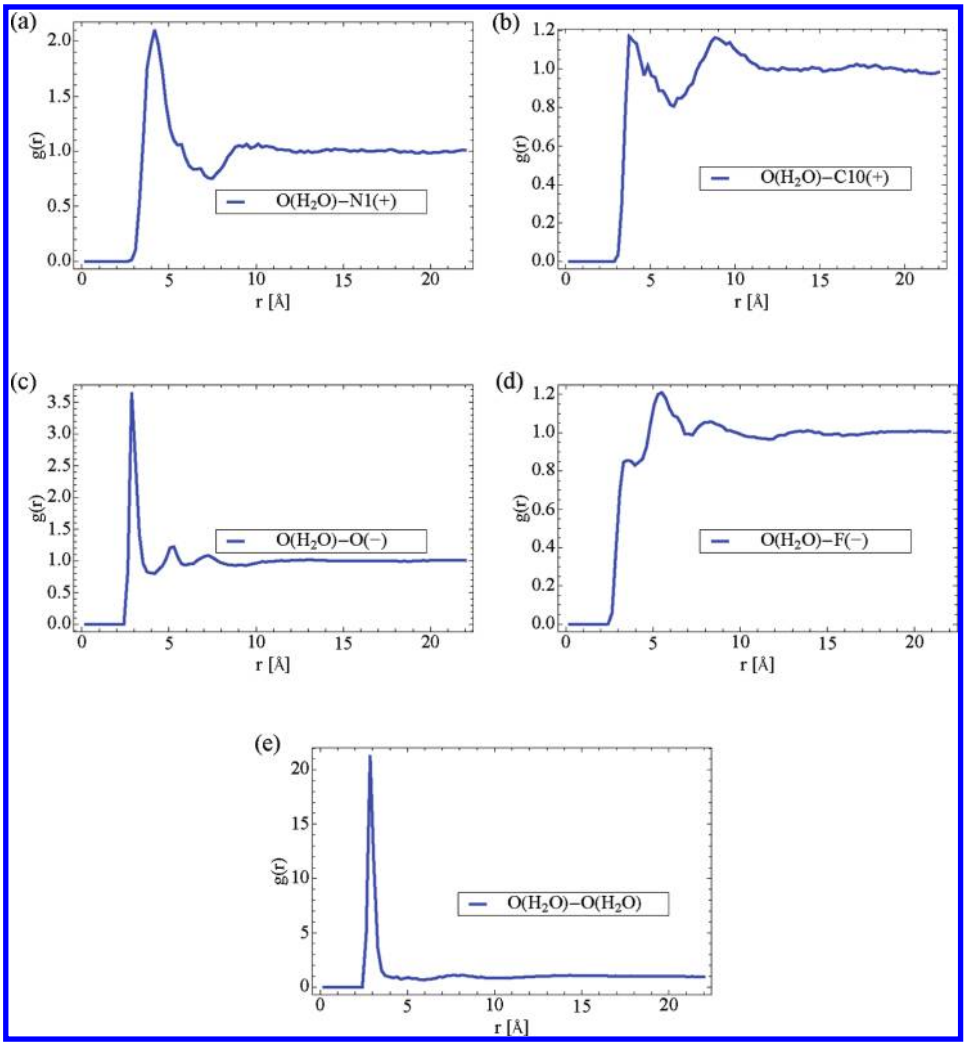

Figure 9. Radial distribution functions around $O(H_2O)$, in the pseudobulk region of the IL/H_2O system.

The increased density as well as the angular orientation of the contact pairs is indicative of increased intermolecular interactions that exert a lateral tension in the plane of the interface. This would be expected to affect the surface tension.

For the C2(+)−O(−) pair in the IL−CO_2 system, the aCP and mCP counts were 129.8 and 112.6%. This is slightly less than that for the IL/vacuum case. The density profile and angular distribution plots for the C2(+)−O(−) CPs are shown in Figure 13. CO_2 has an interesting effect on the CP density; most of the reduction in CP density, responsible for lowering the overall CP count, happens at the interfaces. The height of the interfacial peak in density is reduced compared with that of the IL/vacuum system. This suggests that CO_2 reduces the surface tension because it breaks up the CP association. In a later section, we will discuss surface tension results and see that this is in fact the case. The main features of the angular distribution of the CPs remain unchanged.

In the IL/H_2O system, analysis of CPs was performed for C2(+)−O(−) and $O(H_2O)$−O(−) pair types. The number of C2(+)−O(−) aCPs and mCPs is 125.5 and 109.2%, indicating that H_2O disrupts CPs more than CO_2. Figure 14 shows that in this case the decrease in CP density is not just at the interface but also in the pseudobulk region. Correspondingly, the surface tension is not expected to be altered much by H_2O as compared with CO_2.

The number of $O(H_2O)$−O(−) CPs was quite high in the IL/H_2O system, at 140.9 and 127.6% for aCPs and mCPs. There is no density or orientational preference. The mCP count indicates that ∼1/3 of the H_2O molecules are interacting with two anions at any given time. The aCP count, which is even higher, shows that some of the H_2O molecules are interacting with multiple oxygens on the same anion. This demonstrates that the H_2O associates very strongly with the IL and even helps bind multiple ions together.

In the IL/H_2O/CO_2 system, the C2(+)−O(−) CP counts were 121.1 and 105.8%. The CP density profile (not shown) has lowered CP density peaks at the interface as well as lower CP density in the bulk. The lower CP values are the result of the combined effect of the CO_2 reducing the CP density peaks at the interface as well as the H_2O reducing the CP density in the bulk.

Dynamics. Mean square displacements (MSDs) for IL and solute molecules were computed only for molecules and ions in the "pseudo-bulk" region. This was done by applying the standard method for MSDs[27] but only to the molecules whose trajectories remained in the "pseudo-bulk" region for the entire

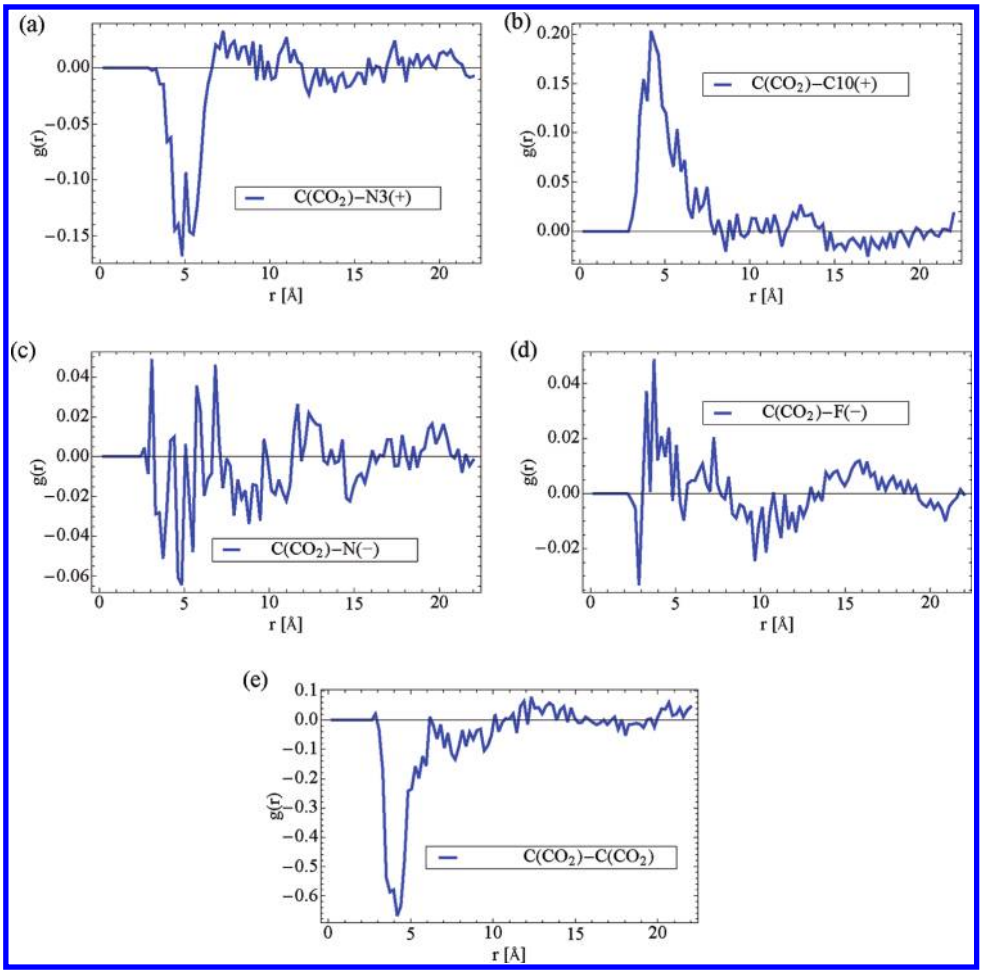

Figure 10. Differences in the radial distribution functions around $C(CO_2)$ between the IL/CO_2 and $IL/H_2O/CO_2$ systems in the pseudobulk region.

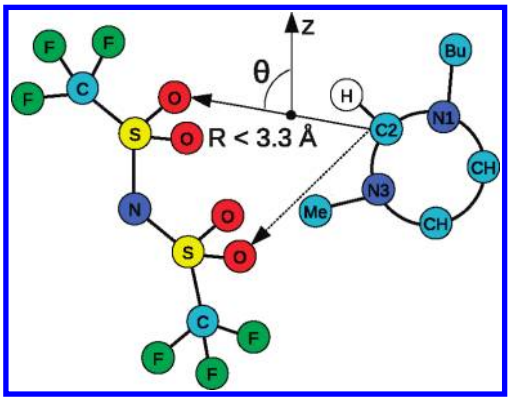

Figure 11. Criteria for identifying atom contact pairs (aCPs) and molecule contact pairs (mCPs). The solid arrow going from C2(+) to O(−) represents a vector with length $R < 3.3$ Å between that atom pair, indicating an aCP. The solid arrow labeled "z" is the z axis, which is parallel to the interface normal, and the angle between the aCP vector and the interface normal is θ. The dotted arrow represents a second aCP between a different pair of atoms on the same molecule pair. The second aCP (and any additional aCPs occurring between the same molecule pair) is ignored in the count of mCPs.

time over which the correlation was calculated. The x and y components of the MSD were averaged, whereas the z component of the MSD was discarded because the interfaces constrain the motion of the ions and make the z component anomalously low.

The xy average MSDs in the IL/vacuum, IL/CO_2, IL/H_2O, and $IL/H_2O/CO_2$ systems are shown in Figure 15. The MSDs appear to be linear, suggesting diffusive motion. The MSD of the cation is shown in Figure 15a, and the MSD of the anion is shown in Figure 15b. Figure 15c shows the MSD for CO_2 in the IL/CO_2 and $IL/H_2O/CO_2$ systems. Figure 15d shows the MSD of H_2O in the IL/H_2O and $IL/H_2O/CO_2$ systems. The MSDs of the cation and anion are slightly higher in the IL/CO_2 system than for the IL/vacuum system, although the difference is small. Note that the CO_2 diffuses much more rapidly than the IL molecules.

The diffusion of the cation and anion in the IL/H_2O system is reduced compared with the IL/CO_2 and IL/vacuum systems, indicating that H_2O slows down the bulk diffusion. Also, the diffusion of CO_2 in the $IL/H_2O/CO_2$ case has been slowed down by H_2O compared with the IL/CO_2 case. Comparing the MSDs for all of the systems, it can be observed that the H_2O has the effect of greatly slowing down the diffusion, whereas CO_2 seems to slightly increase it. Possible explanations for this behavior are given in the next section.

Interfacial crossing dynamics can be characterized in terms of residence time distributions (RTDs) and crossing time distributions (CTDs). A region consisting of a 10 Å slab of IL at the interface with a 10 Å slab of gas was defined as the interfacial region. Four modes of transit with respect to the interface were

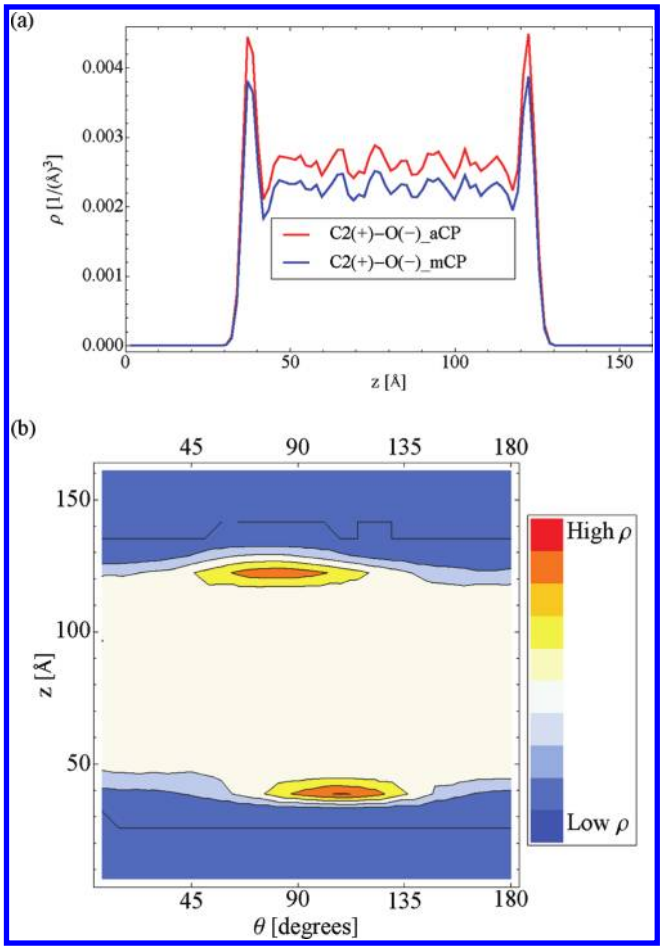

Figure 12. Density profile (a) and angular distribution (b) of the C2(+)−O(−) contact pairs in the IL/vacuum system.

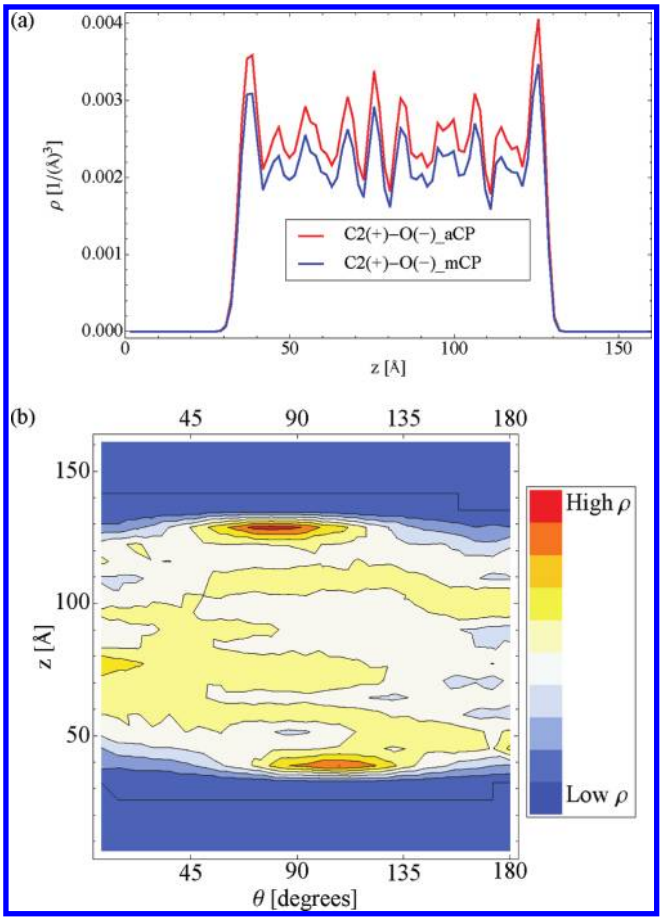

Figure 13. Density profile (a) and angular distribution (b) of the C2(+)−O(−) contact pairs in the IL/CO_2 system.

defined. When a molecule enters the interfacial region from the gas and then exits back into the gas, a "gas-to-gas" (GTG) event occurs. Similarly a "liquid-to-liquid" (LTL) event corresponds to a molecule entering from and then exiting back into the liquid, and "gas-to-liquid" (GTL) and "liquid-to-gas" (LTG) events correspond to a molecule crossing through the interfacial region from the gas into the liquid and from the liquid into the gas. In all cases, the time that the molecule spent in the interfacial slab was recorded, and for each case, a time distribution histogram was created from all of the events that occurred during the simulation. The time distributions for the GTG and LTL events are considered to be RTDs, and the distributions for the GTL and LTG events are considered to be CTDs.

The interfacial RTD and CTD for CO_2 in the IL/CO_2 system and in the IL/H_2O/CO_2 system are shown in the Supporting Information. These interfacial RTDs and CTDs are very similar for the IL/CO_2 and IL/H_2O/CO_2 systems. H_2O has little effect on this aspect of the interfacial transport behavior.

It was expected that H_2O would disrupt the ion−ion interactions and cause the dynamics to speed up, but instead the opposite was observed. The next section shows how some of the behavioral tendencies of the H_2O molecules may explain the reduction in dynamics.

Behavior of H_2O in the IL. The O(H_2O)−O(−) CP values show that the H_2O molecules interact with multiple anions at once, effectively tying them together and having the surprising effect of slowing dynamics such as diffusion. If the H_2O molecules are interacting with multiple O(−)s on the same anion, this further constrains the motion of the anion, which again slows the dynamics. It was observed by Lynden-Bell and colleagues in dmim-Cl/H_2O mixtures[24] and by Maginn and colleagues[23] in emim-$EtSO_4$/H_2O mixtures that when H_2O is present at low concentrations, it can tie two anions together by forming one hydrogen bond with each. This has also been observed experimentally by Welton and colleagues.[28] Another way to look at this is that by requiring that the anions be positioned in such a way that the atom and molecule CP counts can be satisfied, the configurational space available to the IL is reduced and dynamics are hindered.

Additional insight can be gained by examining the way in which H_2O clusters. Clustering behavior relates to the degree to which H_2O associates with itself in the dilute solution. A cluster is defined as a collection of H_2O molecules whose oxygens atoms are within a 4 Å radius. Clusters can consist of two or more H_2O molecules. The number of molecules in a cluster as well as the center of mass (COM) of the cluster were computed. Cluster size distributions and density profiles in z of cluster COMs were also created.

Figure 16a shows the cluster size distribution of H_2O molecules for the IL/H_2O system. Figure 16b shows the density profile of single (unclustered) H_2O molecules, cluster COMs for clusters of size 2, 3, and >3, and the overall water density. The

majority of the H_2O molecules are unclustered, although there are a substantial number of H_2O pairs and smaller numbers of larger clusters. This is in agreement with previous studies of IL/H_2O systems.[13,14] Clustering behavior does not seem to be affected by proximity to the interface, but rather clusters occur at a greater density where the H_2O density is higher.

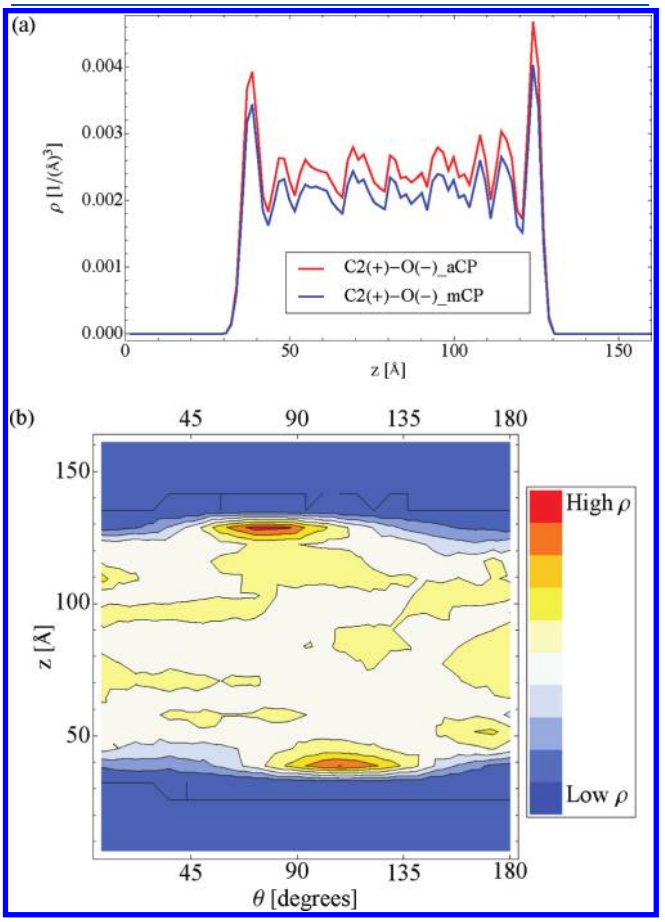

Figure 14. Density profile (a) and angular distribution (b) of the C2(+)−O(−) contact pairs in the IL/H_2O system.

It might be expected that the H_2O would have the effect of solvating the IL ions, which would disrupt the cation−anion interactions and increase dynamics. The H_2O molecules for the most part are isolated or in pairs because of their low concentration and so are not able to solvate the IL ions. Nevertheless, they are able to form many associations with the ions. It appears that the isolated H_2O molecules are small enough to fit into the interstices between the ions, thereby having only a minimal disruption on the cation−anion interactions while at the same time interacting with multiple anions and tying them together (as described above), which slows the dynamics overall. At sufficiently high concentrations of H_2O, we would expect to see that the H_2O molecules form solvation shells around the ions. Given that fewer H_2O molecules interact with multiple anions at a time, this should result in an increase in the dynamics.

The conclusion that small amounts of H_2O actually slow the dynamics is unverified experimentally; therefore, this is a tentative conclusion. This phenomenon may be the result of the type of H_2O model that is used. The SPC model was developed to capture the behavior of bulk H_2O. As such, it has a large fixed dipole moment due to the fact that H_2O is highly polarized in the high dielectric medium of bulk H_2O. In an IL phase where the dielectric constant is thought to be much lower,[29,30] the actual dipole moment of H_2O may be lower, and it would therefore interact less strongly with the anions. Additional work on this is warranted.

Surface Tension. Surface tension was computed from the diagonal components of the virial tensor, averaged over the entire 12 ns production run.[27] Block averages of the surface tension values were computed and used to compute the standard deviations of the surface tensions. Note that the standard deviations are quite large, as is typical for this type of calculation.

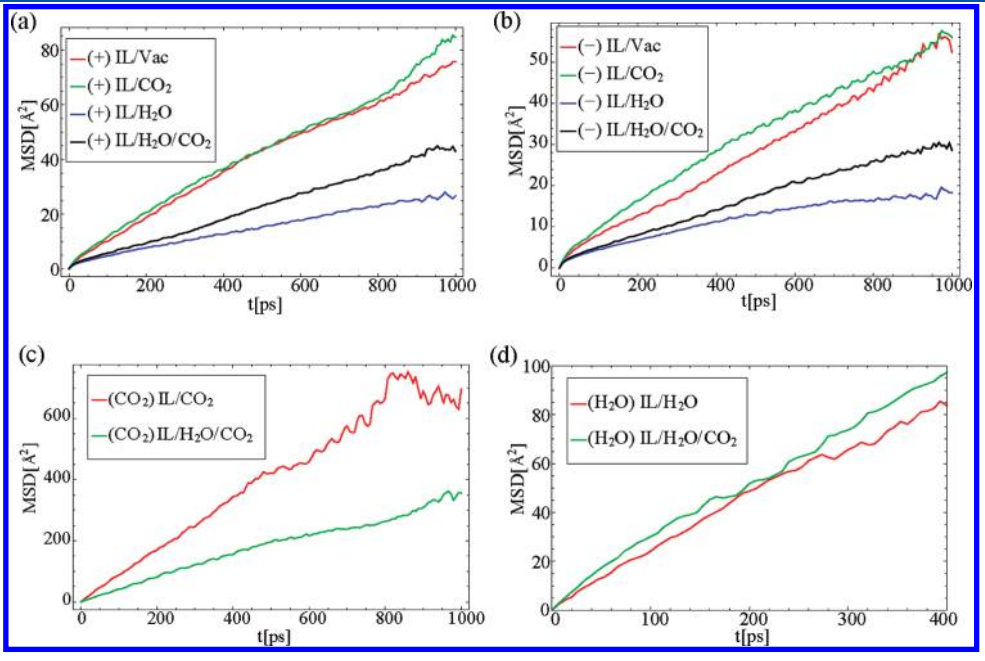

Figure 15. MSD plots for the cation (a), anion (b), CO_2 (c), and H_2O (d) in the IL/vacuum, IL/CO_2, IL/H_2O, and IL/H_2O/CO_2 systems.

dx.doi.org/10.1021/jp203838j |J. Phys. Chem. B 2011, 115, 10488–10499

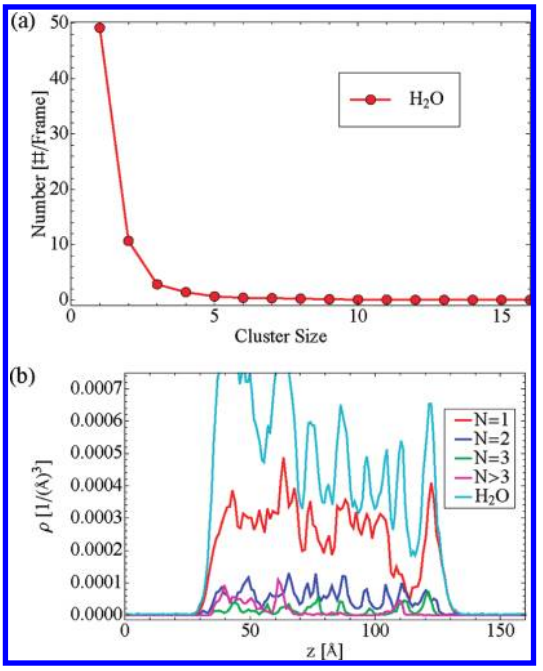

Figure 16. Clustering behavior of H_2O in the IL/H_2O system. (a) Average number of H_2O clusters of different sizes. (b) Density profiles of the COMs of clusters of different sizes. $N = 1$ through $N > 3$ indicate profiles for clusters with N number of H_2O molecules; $N = 1$ corresponds to single (unclustered) H_2O molecules. Also shown is the overall density of H_2O.

Table 1. Computed Surface Tensions for Different Cases[a]

system	surface tension [N/m]
IL/vacuum	0.030 (0.021)
IL/192CO_2	0.022 (0.016)
IL/96H_2O	0.034 (0.020)
IL/96H_2O/192CO_2	0.022 (0.019)

[a] Uncertainty is the block average standard deviation.

Table 1 shows the surface tensions calculated for the different interfacial systems as well as the standard deviation. The computed surface tension for the IL/vacuum system is similar to the value of 0.0324 N/m computed by Padua and colleagues[4] for hmim-Tf_2N. The IL/vacuum surface tension also is in the same range as experimental values[31,32] for various $C_n$mim-Tf_2N ILs. Balasubramanian and colleagues[5] also computed surface tensions for C_3C_1im-, C_3C_3im-, C_5C_1im-, and C_5C_5im-Tf_2N ILs. Their values are all in the range of 0.02 to 0.025 N/m, which also are comparable to our values. The CO_2 has a stabilizing effect on the interface, reducing the surface energy (surface tension). H_2O does not seem to have this effect.

The surface tension calculation by Padua and colleagues includes a calculation of surface tension versus depth. Whereas the majority of the contribution to the surface tension is at the interface, in some cases, the pseudobulk region in the center also contributes to the surface tension. This indicates that certain aspects of the interfacial behavior extend deeper into the bulk.[4] In our work, we see that the density oscillations of the cation and anion, which indicate an effect of the interface, extend to the center of the slab, which means that the slab is not thick enough to achieve true bulk behavior in the center. Because true bulk behavior is not exhibited in the center of the slab, we cannot be sure that we have captured all contributions to the surface tension arising from deeper into the liquid; therefore, the surface tension values may not be quantitatively accurate. However, they do seem to show a qualitative trend in the effect of additional components on surface tension.

The energy reducing effect of CO_2 is not surprising given that the high density adsorbed layer of CO_2 at the interface indicates that the IL at the interface and CO_2 have a high affinity for each other. Also, it makes sense that because CO_2 seems to disrupt the intermolecular interactions at the interface (as demonstrated by the reduction of C2(+)−O(−) CPs) the surface tension would be lower. Another way to look at this is that the interface is stabilized by the presence of CO_2, and the result is that the IL molecules interact more with the CO_2 and less with other IL molecules, reducing the C2(+)−O(−) CP density.

The surface tension has been measured experimentally at different pressures of CO_2 for bmim-PF_6 and bupy-BF_4,[33] and for emim-[2-(2-ethoxyethoxy)-ethylsulfate] and bmim-[2-(2-methoxyethoxy)-ethylsulfate].[34] It was observed experimentally that surface tension drops linearly with pressure until a saturation point is reached at ~7 mPa. The proposed mechanism for the reduction in surface tension is that the difference in density across the interface decreases with pressure (because the compressibility of the gas phase is much higher). Because the surface tension is proportional to the gradient normal to the interface of the square of the density difference, surface tension drops.

In a previous computational study, we observed that the density of the adsorbed layer of CO_2 as well as the bulk solubility is linear with pressure. Experiment shows that surface tension decreases linearly with pressure[33,34] until the IL is saturated with CO_2. This may indicate that surface tension is dependent on the adsorption/absorption of CO_2. Furthermore, our current work suggests that the observed decrease is at least partially the result of the specific interactions that take place between the IL and CO_2 at the interface. So it appears from our current work that the adsorbed layer of CO_2 and the manner in which it interacts with the IL has an additional effect on the surface tension.

H_2O, however, does not have an affinity for the interface. In fact, the H_2O is almost completely in the bulk, and the interfacial density is close to zero. Therefore, it makes sense that adding H_2O to the system has little effect on the surface energy. If H_2O was present in the vapor phase at substantially higher density (which would require a higher temperature so that the vapor pressure of H_2O could be higher), then possibly there would be a significant amount of H_2O at the interface, maybe even an adsorbed layer, as seen with the CO_2, and possibly the presence of H_2O at the interface would affect the interfacial energy.

CONCLUSIONS

Results of MD simulations of the bmim-Tf_2N/vacuum, bmim-Tf_2N/H_2O, bmim-Tf_2N/CO_2, and bmim-Tf_2N/H_2O/CO_2 interfaces at 350 K have been reported. H_2O exhibits a set of interfacial ordering tendencies distinct from the behavior exhibited by CO_2. It absorbs completely into the IL and avoids the interface.

H_2O associates strongly with the anion and also to some degree with itself, exhibiting a tendency to form pairs. There is also a strong association between the C2(+) and O(−) sites in all IL systems. At the interface, there is an increased density of these

interactions, and the C2(+)−O(−) pair vectors are primarily aligned with the plane of the interface. This is presumed to be one mechanism from which surface tension arises. The presence of CO_2 adsorbed on the surface disrupts the C2(+)−O(−) associations, with a corresponding reduction in interfacial tension. H_2O does not have this effect.

Diffusive dynamics are not strongly affected by CO_2. However H_2O slows the diffusion of both IL and CO_2 molecules. The reduction of diffusion by H_2O is attributed to the strong interaction of H_2O molecules with multiple anion molecules, which constrains their motion, and to the inability of H_2O molecules to solvate effectively the IL ions on account of being mostly isolated or in pairs. The presence of H_2O in solution has little effect on the interfacial transport dynamics of CO_2.

■ ASSOCIATED CONTENT

Supporting Information. RTD and CTD plots are provided in the Supporting Information. This material is available free of charge via the Internet at http://pubs.acs.org.

■ AUTHOR INFORMATION

Corresponding Author
*E-mail: ed@nd.edu.

■ ACKNOWLEDGMENT

Computational resources were provided by the Notre Dame Center for Research Computing. Marcos E. Perez-Blanco acknowledges financial support of the Lilly Fellowship. This material is based on work supported by the Department of Energy under award number DE-FC26-07NT43091.

■ REFERENCES

(1) Anthony, J. L.; Maginn, E. J.; Brennecke, J. F. *J. Phys. Chem. B* **2002**, *106*, 7315.
(2) Dyson, P. J.; Laurenczy, G.; Ohlin, C. A.; Vallance, J.; Welton, T. *Chem. Commun.* **2003**, 2418.
(3) Perez-Blanco, M. E.; Maginn, E. J. *J. Phys. Chem. B* **2010**, *114*, 11827–11837.
(4) Pensado, A. S.; Malfreyt, P.; Padua, A. A. H. *J. Phys. Chem. B* **2009**, *113*, 14708–14718.
(5) Sarangi, S. S.; Raju, S. G.; Balasubramanian, S. *Phys. Chem. Chem. Phys.* **2011**, *13*, 2714–2722.
(6) Wick, C. D.; Chang, T.-M.; Dang, L. X. *J. Phys. Chem. B* **2010**, *114*, 14965–14971.
(7) Dang, L. X.; Wick, C. D. *J. Phys. Chem. B* **2011**, *115*, 6964–6970.
(8) Nishi, N.; Yasui, Y.; Uruga, T.; Tanida, H.; Yamada, T.; Nakayama, S.; Matsuoka, H.; Kakiuchi, T. *J. Chem. Phys.* **2010**, *132*, 164705.
(9) Roscioli, J. R.; Nesbitt, D. J. *J. Phys. Chem. Lett.* **2010**, *1*, 674–678.
(10) Lynden-Bell, R. M.; Kohanoff, J.; Del Popolo, M. G. *Faraday Discuss.* **2005**, *129*, 57.
(11) Lynden-Bell, R. M. *Mol. Phys.* **2003**, *101*, 2625.
(12) Annapureddy, H. V. R.; Hu, Z.; Xia, J.; Margulis, C. J. *J. Phys. Chem. B* **2008**, *112*, 1770–1776.
(13) Moreno, M.; Castiglione, F.; Mele, A.; Pasqui, C.; Raos, G. *J. Phys. Chem. B* **2008**, *112*, 7826–7836.
(14) Hanke, C. G.; Lynden-Bell, R. M. *J. Phys. Chem. B* **2003**, *107*, 10873–10878.
(15) Jiang, W.; Wang, Y.; Voth, G. A. *J. Phys. Chem. B* **2007**, *111*, 4812–4818.
(16) Cadena, C.; Anthony, J. L.; Shah, J. K.; Morrow, T. I.; Brennecke, J. F.; Maginn, E. J. *J. Am. Chem. Soc.* **2004**, *126*, 5300.
(17) MacKerell, A. D., Jr.; Bashford, D.; Bellott, M.; Dunbrack, R. L., Jr.; Evanseck, J. D.; Field, M. J.; Fischer, S.; Gao, J.; Guo, H.; Ha, S.; Joseph-McCarthy, D.; Kuchnir, L.; Kuczera, K.; Lau, F. T. K.; Mattos, C.; Michnick, S.; Ngo, T.; Nguyen, D. T.; Prodhom, B.; Reiher, W. E.; Roux, B.; Schlenkrich, M.; Smith, J. C.; Stote, R.; Straub, J.; Watanabe, M.; Wiórkiewicz-Kuczera, J.; Yin, D.; Karplus, M. *J. Phys. Chem. B* **1998**, *102*, 3586–3616 .
(18) Lopes, J. N. C.; Padua, A. A. H. *J. Phys. Chem. B* **2004**, *108*, 16893.
(19) Potoff, J. J.; Siepmann, J. I. *AIChE J.* **2001**, *47*, 1676.
(20) Tironi, I. G.; Brunne, R. M.; van Gunsteren, W. F. *Chem. Phys. Lett.* **1996**, *250*, 19–24.
(21) Plimpton, S. J. *J Comp Phys* **1995**, *117*, 1.
(22) LAMMPS Molecular Dynamics Simulator. http://lammps.sandia.gov/ (accessed Jan 9, 2009).
(23) Kelkar, M. S.; Shi, W.; Maginn, E. J. *Ind. Eng. Chem. Res.* **2008**, *47*, 9115–9126.
(24) Hanke, C. G.; Atamas, N. A.; Lynden-Bell, R. M. *Green Chem.* **2002**, *4*, 107–111.
(25) Lopes, J. N. C.; Gomes, M. F. C.; Padua, A. A. H. *J. Phys. Chem. B* **2006**, *110*, 16816–16818.
(26) Mark, P.; Nilsson, L. *J. Phys. Chem. A* **2001**, *105*, 9954–9960.
(27) Frenkel, D.; Smit, B. *Understanding Molecular Simulation: From Algorithms to Applications*, 2nd ed.; Academic Press: San Diego, 2002.
(28) Cammarata, L.; Kazarian, S. G.; Salter, P. A.; Welton, T. *Phys. Chem. Chem. Phys.* **2001**, *3*, 5192–5200.
(29) Weingartner, H.; Knocks, A.; Schrader, W.; Kaatze, U. *J. Phys. Chem. A* **2001**, *105*, 8646–8650.
(30) Wakai, C.; Oleinikova, A.; Ott, M.; Weingartner, H. *J. Phys. Chem. B* **2005**, *109*, 17028–17030.
(31) Zaitsau, D. H.; Kabo, G. J.; Strechan, A. A.; Paulechka, Y. U.; Tschersich, A.; Verevkin, S. P.; Heintz, A. *J. Phys. Chem. A* **2006**, *110*, 7303–7306.
(32) Carvalho, P. J.; Freire, M. G.; Marrucho, I. M.; Queimada, A. J.; Coutinho, J. A. P. *J. Chem. Eng. Data* **2008**, *53*, 1346–1350.
(33) Jaeger, P.; Eggers, R. *Chem. Eng. Process.* **2009**, *48*, 1173–1176.
(34) Hebach, A.; Oberhof, A.; Dahmen, N.; Griesheimer, P. *J. Chem. Eng. Data* **2009**, *54*, 1249–1253.